Struct Multidisc Optim (2006) 31: 96–104
DOI 10.1007/s00158-005-0540-2

RESEARCH PAPER

J. X. Zhou · X. M. Wang · Z. Q. Zhang · L. Zhang

On the enhancement of computation and exploration of discretization approaches for meshless shape design sensitivity analysis

Received: 4 June 2004 / Revised manuscript received: 17 March 2005 / Published online: 23 November 2005

Abstract A new implementation of Reproducing Kernel Particle Method (RKPM) is proposed to enhance the process of shape design sensitivity analysis (DSA). The acceleration process is accomplished by expressing RKPM shape functions and their derivatives explicitly in terms of kernel function moments. In addition, two different discretization approaches are explored elaborately, which emanate from discretizing design sensitivity equation using the direct differentiation method. Comparison of these two approaches is made, and the equivalence of these two superficially different approaches is demonstrated through two elastostatics problems. The effectiveness of the enhanced RKPM is also verified by comparison of consumption of computer time between the classical method and the improved method.

Keywords Design sensitivity analysis · Shape optimization · Meshless method · Discretization

1 Introduction

The term shape optimization is often used in a narrow sense referring only to the optimal design of the shape of the boundary of 2D and 3D structural components. The twin term design sensitivity analysis (DSA), that is, the calculation of quantitative information on how the responses of a structure is affected by changes in the variables that define its shape, is a fundamental requirement for shape optimization (Haftka and Grandhi 1986). Major computational challenges involved in shape design optimization using finite element method (FEM) arise from mesh distortion that occurs during large shape design changes, potentially many times of re-meshing that are needed during the optimization process, and the difficulties in sensitivity calculation stemming from inaccurate boundary representation and inaccurate boundary solutions. The recently developed meshless or meshfree methods (Belytschko et al. 1994, 1996; Liu et al. 1995, 1996; Duarte and Oden 1995; Melenk and Babuska 1999; Li and Liu 2002; Atluri and Zhu 2000), on the other hand, overcome the aforementioned major drawbacks of the FEM and seem to be ideally suited for boundary shape optimization. Meshless methods can provide higher rates of convergence than the FEM as well as more accurate boundary solutions. They can also provide continuous structural responses such as strain and stress at no additional cost. This is of great importance in sensitivity calculation because special strategy for smoothing of structural responses is avoided. Moreover, using the element-free Galerkin (EFG) method, Bobaru and Mukherjee (2001) have shown that the solution given by EFG is rather insensitive with respect to the arrangement of the nodes. Therefore, an optimization procedure for the position of nodes seems unnecessary. For all these reasons, meshless methods seem to constitute very appealing approaches for sensitivity analysis and shape optimization.

There are several published researches which use meshless method as a tool for structural analysis and sensitivity analysis. Grindeanu et al. (1998) used Reproducing Kernel Particle Method (RKPM) for DSA of hyperelastic structures. Various 1D and 3D examples were presented to demonstrate the feasibility and accuracy of RKPM for DSA. It is shown that mesh distortion or entanglement encountered in large deformation and shape design optimization is eliminated completely. Kim et al. (2000a, 2000b, 2001) introduced meshless method into the shape design optimization problems with emphasis on the contact problem of nearly incompressible hyperelastic material and elasto-plasticity. Bobaru and Mukherjee (2001) applied EFG method to shape DSA and shape optimization problems in 2D elasticity. A new discretization approach was proposed, and the displacement sensitivity equation was discretized directly avoiding differentiation of the EFG shape functions. Smoother stresses and better accuracy for points close to the boundary are obtained by EFG as compared to published results using the FEM, the boundary element method, or the boundary contour method. Recently, Kim et al. (2003) presented some 2D and 3D shape optimization examples by RKPM. It is shown that the number of design iterations is reduced because of the accurate sensitivity information given by the meshless method.

J. X. Zhou (✉) · X. M. Wang · Z. Q. Zhang · L. Zhang
School of Civil Engineering and Mechanics,
Xi'an Jiaotong University, Xi'an, 710049,
People's Republic of China
e-mail: jxzhouxx@xjtu.edu.cn

For the gradient-based optimization algorithm, an accurate evaluation of sensitivity information is a crucial point of the entire optimization procedure. Efficient and accurate sensitivity computation, with respect to shape design parameters, can substantially reduce the design optimization costs. Unfortunately, one of the main drawbacks of meshless method lies in the fact that construction of shape functions and their derivatives is more time-consuming as compared to the FEM. Any improvement or enhancement of the efficiency of meshless method leads to the acceleration of meshless analysis and ultimately the enhancement of sensitivity analysis, which is of great value for shape optimization and shape sensitivity analysis. For this reason, effort is motivated to enhance the computation of meshless method shape functions and their derivatives. For the specific Galerkin meshless method, RKPM, this enhancement is realized through a new implementation of RKPM, i.e., expressing explicitly RKPM shape functions in terms of kernel function moments. This avoids matrix inversions or solutions of linear systems, which are involved in classical RKPM procedure. The effectiveness of enhanced RKPM is demonstrated through two 2D linear elasticity shape DSA problems by comparison of computer time between classical RKPM and the improved RKPM. Recently, the authors have developed this enhancement strategy further into a 3D case, and a speedup of computation is also observed in 3D structural analysis (Zhou et al. 2005).

Summarizing the available literature with reference to meshless shape DSA using material derivative and direct differentiation method (DDM), there are two apparently different discretization approaches, which are employed in the meshless discretization of design sensitivity equation. Kim et al. (2003) emphasize the difference between the FEM shape functions and meshless shape functions: FEM shape functions depend on the parent geometry of the element, which is fixed throughout the design variations; while the shape functions of meshless method hinge on global coordinates of material points that are the design parameters for shape DSA. Therefore, the material derivative of meshless shape functions, which explicitly depends on design velocity, has to be considered in approximating sensitivity of displacement and sensitivities of other derived variables. Alternatively, Bobaru and Mukherjee (2001) consider the sensitivity of displacement as a common continuous function, and approximate it directly by a standard Galerkin procedure without introducing material derivative of shape functions. The former discretization approach (we call it Kim's approach in this paper) is more consistent in the sense of discretization, but the latter (Bobaru's approach) is definitely correct and particularly simplifies the implementation of shape DSA by meshless method. These two discretization approaches are examined carefully, and the equivalence of these two approaches is shown clearly by two numerical examples.

The outline of the paper is as follows: the classical RKPM is overviewed briefly, and the enhanced RKPM is proposed in Section 2. The improved RKPM is applied to DSA, and two discretization schemes for approximating sensitivity equation are explored in Section 3. Two DSA problems and a portal frame shape optimization problem are given in Section 4 to demonstrate the effectiveness of the enhancements. Lastly, some concluding remarks are made in Section 5.

2 Highlights of RKPM for structural analysis

2.1 Enhanced RKPM for efficient computation of shape functions

For the purpose of illustration, the 2D elasticity problem is chosen here to show the enhancement of classical RKPM, in which the shape functions and their first derivatives have the following form:

$$N_I(x,y) = [c_0 + c_1(x-x_I) + c_2(y-y_I)]w_d(x,y) \tag{1}$$

$$N_{I,x}(x,y) = [c_{0,x} + c_{1,x}(x-x_I) + c_1 + c_{2,x}(y-y_I)]w_d(x,y) + [c_0 + c_1(x-x_I) + c_2(y-y_I)]w_{d,x}(x,y) \tag{2}$$

$$N_{I,y}(x,y) = [c_{0,y} + c_{1,y}(x-x_I) + c_2 + c_{2,y}(y-y_I)]w_d(x,y) + [c_0 + c_1(x-x_I) + c_2(y-y_I)]w_{d,y}(x,y) \tag{3}$$

where $N_I(x,y)$, $N_{I,x}(x,y)$, and $N_{I,y}(x,y)$ are the shape function associated with node I and its derivatives with respect to x and y, respectively; $w_d(x,y)$ is the kernel function and is chosen as the cubic spline function in this paper; c_i, $c_{i,x}$, and $c_{i,y}$ are correction coefficients, derivatives of correction coefficients with respect to x and y, respectively. In classical RKPM implementation, the correction coefficient vector $\overline{\mathbf{C}}$ and its derivatives $\overline{\mathbf{C}}_{,x}$ and $\overline{\mathbf{C}}_{,y}$ are obtained by solving the so-called reproducing conditions, i.e., the following 9×9 simultaneous equations:

$$\begin{bmatrix} \mathbf{M} & \mathbf{0} & \mathbf{0} \\ \mathbf{M}_{,x} & \mathbf{M} & \mathbf{0} \\ \mathbf{M}_{,y} & \mathbf{0} & \mathbf{M} \end{bmatrix} \begin{bmatrix} \overline{\mathbf{C}} \\ \overline{\mathbf{C}}_{,x} \\ \overline{\mathbf{C}}_{,y} \end{bmatrix} = \begin{bmatrix} \overline{\mathbf{M}} \\ \mathbf{0} \\ \mathbf{0} \end{bmatrix} \tag{4}$$

where $\mathbf{M}$ is the 3×3 moment coefficient matrix, $\mathbf{M}_{,x}$ and $\mathbf{M}_{,y}$ are derivatives of $\mathbf{M}$ with respect to x and y, and $\overline{\mathbf{M}}$ is the 3×1 known right-hand vector. Solving (4) may involve matrix inversions or solutions of linear equations, which exhausts most of computer time when frequent shape functions constructions are needed.

Motivation is inspired by the fact that the analytical solution of (4), in terms of kernel function moments, are obtainable provided that analytical form of inversion of matrix $\mathbf{M}$ is derived. This is not a difficult task, and the ex-

plicit forms of correction coefficients and their derivatives are summarized as follows:

$$c_i = v_{i0}/\Delta \qquad (i = 0,\ 1,\ 2) \tag{5}$$

$$\begin{aligned} c_{i,x} = -\frac{1}{\Delta^2}[&v_{00}(v_{i0}m_{00,x} + v_{i1}m_{10,x} + v_{i2}m_{01,x}) \\ &+ v_{10}(v_{i0}m_{10,x} + v_{i1}m_{20,x} + v_{i2}m_{11,x}) \\ &+ v_{20}(v_{i0}m_{01,x} + v_{i1}m_{11,x} + v_{i2}m_{02,x})] \end{aligned} \tag{6}$$

where

$$\begin{aligned} v_{00} &= m_{02}m_{20} - m_{11}^2 \\ v_{10} &= v_{01} = m_{01}m_{11} - m_{02}m_{10} \\ v_{20} &= v_{02} = m_{10}m_{11} - m_{01}m_{20} \\ v_{11} &= m_{00}m_{02} - m_{01}^2 \\ v_{12} &= v_{21} = m_{01}m_{10} - m_{00}m_{11} \\ v_{22} &= m_{00}m_{20} - m_{10}^2 \end{aligned}$$

and

$$\begin{aligned} \Delta = &m_{00}m_{20}m_{02} + m_{10}m_{11}m_{01} + m_{01}m_{10}m_{11} \\ &- m_{01}^2 m_{20} - m_{10}^2 m_{02} - m_{11}^2 m_{00} \end{aligned}$$

m_{ij} are kernel function moments in the following form for the 2D problem considered herein:

$$\begin{aligned} m_{ij}(x, y) = \int_\Omega &(x - s)^i (y - t)^j \times \\ &w_d(x - s, y - t)\mathrm{d}s\mathrm{d}t \end{aligned} \tag{7}$$

Substituting expressions (5) and (6) into (1)–(3) gives explicit RKPM shape functions in terms of kernel function moments. Enhancement of RKPM is the consequence of the fact that frequent matrix inversions or solutions of linear systems are replaced by the much cheaper algebraic manipulations in (5) and (6).

2.1.1 Galerkin meshless discretization

For 2D linear elasticity problem, the principle of virtual work gives, using penalty method to enforce essential boundary conditions, the following weak form:

$$\begin{aligned} &\int_\Omega \sigma \cdot \varepsilon \mathrm{d}\Omega - \int_\Omega \boldsymbol{\eta} \cdot \mathbf{b} d\Gamma - \int_{\Gamma_t} \boldsymbol{\eta} \cdot \bar{\mathbf{t}} d\Gamma + \\ &\alpha \int_{\Gamma_u} \eta \cdot (\mathbf{u} - \mathbf{u})\mathrm{d}\Gamma = 0 \end{aligned} \tag{8}$$

where σ is the stress tensor corresponding to the displacement $\mathbf{u}$, $\mathbf{b}$ is the body force vector, $\bar{\mathbf{t}}$ is the traction on the Γ_t part of the boundary of Ω with normal $\mathbf{n}$, and $\overline{\mathbf{u}}$ is the prescribed displacement on the boundary Γ_u. Applying Galerkin approximations via RKPM shape functions to trial function $\mathbf{u}$ and test function η yields

$$\mathbf{u} = \sum_{I=1}^{\mathrm{NP}} N^I \mathbf{d}^I,\ \eta = \sum_{I=1}^{\mathrm{NP}} N^I \tilde{\mathbf{d}}^I \tag{9}$$

where NP denotes the total number of particles, $\mathbf{d}^I$ designates the generalized displacement vector of particle I, and similarly for $\tilde{\mathbf{d}}^I$. Substituting approximation (9) into (8) gives, referring to (Bobaru and Mukherjee 2001) for detailed expressions of $\mathbf{K}$, $\mathbf{K}_\alpha$, $\mathbf{F}$ and $\mathbf{F}_\mathrm{a}$, the following discrete equations:

$$(\mathbf{K} + \mathbf{K}_\alpha)\mathbf{d} = \mathbf{F} + \mathbf{F}_\mathbf{a} \tag{10}$$

where $\mathbf{d}$ is the global generalized displacement vector, the matrices $\mathbf{K}$ and $\mathbf{K}_\alpha$ are gathered from the following submatrices

$$\mathbf{K}_{IJ} = \int_\Omega \mathbf{B}_I^\mathrm{T} \mathbf{D} \mathbf{B}_J \mathrm{d}\Omega \tag{11}$$

$$\mathbf{K}_{IJ}^\alpha = \alpha \int_{\Gamma_u} \Phi_I^\mathrm{T} \mathbf{S} \Phi_J \mathrm{d}\Gamma \tag{12}$$

in which

$$\mathbf{B}_i = \begin{bmatrix} \partial N^I/\partial x & 0 \\ 0 & \partial N^I/\partial y \\ \partial N^I/\partial y & \partial N^I/\partial x \end{bmatrix},$$

$$\Phi_I = \begin{bmatrix} N^I & 0 \\ 0 & N^I \end{bmatrix},\ \mathbf{S} = \begin{bmatrix} S_1 & 0 \\ 0 & S_2 \end{bmatrix}$$

S_i is defined so that when u_i is prescribed on Γ_u then S_i=1 and otherwise S_i=0. Similarly, vectors $\mathbf{F}$ and $\mathbf{F}_\mathrm{a}$ consist of the following subvectors

$$\mathbf{F}_I = \int_\Omega \Phi_I^\mathrm{T} \mathbf{b} \mathrm{d}\Omega + \int_{\Gamma_t} \Phi_I^\mathrm{T} \bar{\mathbf{t}} \mathrm{d}\Gamma \tag{13}$$

$$\mathbf{F}_I^\alpha = \beta \int_{\Gamma_u} \Phi_I^\mathrm{T} S \bar{u} \mathbf{d}\Gamma \tag{14}$$

3 Enhanced RKPM for shape DSA

3.1 DDM for the Galerkin weak form using material derivative

Borrowing the material derivative idea from continuum mechanics, the following material derivative or total derivative of displacement with respect to shape design parameter τ is introduced (Haug et al. 1986):

$$\dot{\mathbf{u}} = \lim_{\tau \to 0} \frac{\mathbf{u}_\tau(\mathbf{x} + \tau \mathbf{V}(\mathbf{x})) - \mathbf{u}(\mathbf{x})}{\tau} = \mathbf{u}' + \nabla \mathbf{u} \mathbf{V} \tag{15}$$

where $\mathbf{V}(\mathbf{x})$ is known as the design velocity field. Once the displacement sensitivity as given in (15) is known, the sensitivities of strain and stress are obtained readily as follows:

$$\dot{\varepsilon}(\mathbf{u}) = \varepsilon(\dot{\mathbf{u}}) - \frac{1}{2}\left[\nabla\mathbf{u}\nabla\mathbf{V} + (\nabla\mathbf{u}\nabla\mathbf{V})^{\mathrm{T}}\right] \tag{16}$$

$$\dot{\sigma}(\mathbf{u}) = D : \dot{\varepsilon}(u) \tag{17}$$

In the DDM, we simply take the material derivative of the weak form of the structural (8) and take (15)–(17) into consideration, and ultimately obtain the following so-called design sensitivity equation

$$\begin{aligned}
&\int_\Omega \sigma_{ij}(\dot{u})\varepsilon_{ij}(\eta)\mathrm{d}\Omega + \alpha\int_{\Gamma_u}\eta_i(\dot{u}_i - \dot{\bar{u}}_i)\mathrm{d}\Gamma + \\
&\int_\Omega \sigma_{ij}(\mathbf{u})\varepsilon_{ij}(\eta)\mathrm{div}\mathbf{V}\mathrm{d}\Omega + \int_\Omega \varepsilon^V_{ij}(\eta)\sigma_{ij}(\mathbf{u})\mathrm{d}\Omega \\
&+ \int_\Omega \varepsilon_{ij}(\eta)D_{ijkl}\varepsilon^V_{kl}(\mathbf{u})\mathrm{d}\Omega = \\
&\int_\Omega \eta_i[\dot{b}_i + b_i\mathrm{div}\mathbf{V}]\mathrm{d}\Omega + \int_{\Gamma_t}\eta_i[\dot{\bar{t}}_i + \bar{t}_i(\mathbf{V}\cdot\mathbf{n})H]\mathrm{d}\Gamma - \\
&\alpha\int_{\Gamma_u}\eta_i(u_i - \dot{\bar{u}}_i)(\mathbf{V}\cdot\mathbf{n})H\mathrm{d}\Gamma
\end{aligned} \tag{18}$$

where $H{=}div\mathbf{n}$ is the curvature of o in 2D and the mean curvature of o in 3D, and

$$\varepsilon^V_{ij}(\mathbf{u}) = -\frac{1}{2}\left(\frac{\partial u_i}{\partial x_k}\frac{\partial V_k}{\partial x_j} + \frac{\partial u_j}{\partial x_k}\frac{\partial V_k}{\partial x_i}\right) \tag{19}$$

3.2 Discretizing design sensitivity equation by the Kim's approach

In the Kim's discretization approach, the variation of RKPM shape functions with respect to design variable, i.e., the material derivative of shape functions, is taken into account, and the displacement sensitivity can be approximated as

$$\dot{u} = \sum_{I=1}^{\mathrm{NP}}(N^I\dot{d}^I + \dot{N}^I\mathbf{d}^I) \tag{20}$$

where $\dot{d}^I$ is the material derivative of generalized nodal displacement vector, $\mathbf{d}^I$; $\dot{N}^I$ is the material derivative of shape function. Following the same treatment of shape functions, the material derivative of shape functions is expressed as

$$\begin{aligned}
\dot{N}_I(x,y) = &[\dot{c}_0 + \dot{c}_1(x - x_I) + c_1(V_x - V_x^I) \\
&+ \dot{c}_2(y - y_I) + c_2(V_y - V_y^I)]w_d(x,y) \\
&+ [c_0 + c_1(x - x_I) + c_2(y - y_I)]\dot{w}_d(x,y)
\end{aligned} \tag{21}$$

where the subscripts in V_x and V_y indicate the components of design velocity in the x and y directions, respectively; the superposed dots on the correction coefficients and the kernel function denote the material derivatives of correction functions and kernel function, respectively. The material derivative of kernel function can be obtained easily according to the specific expression of original kernel function. To obtain the material derivative of correction coefficients, a similar reproducing condition as the second equation in (4) can be written as follows

$$\dot{M}\bar{C} + M\dot{\bar{C}} = \mathbf{0} \tag{22}$$

In similar fashion, we can write the analytical form of inversion of matrix $\dot{M}$, and the material derivative of correction coefficients can be expressed in terms of material derivative of kernel function moments in the following form:

$$\begin{aligned}
\dot{c}_i = -\frac{1}{\Delta^2}&[\nu_{00}(\nu_{i0}\dot{m}_{00} + \nu_{i1}\dot{m}_{10} + \nu_{i2}\dot{m}_{01}) \\
&+ \nu_{10}(\nu_{i0}\dot{m}_{10} + \nu_{i1}\dot{m}_{20} + \nu_{i2}\dot{m}_{11}) \\
&+ \nu_{20}(\nu_{i0}\dot{m}_{01} + \nu_{i1}\dot{m}_{11} + \nu_{i2}\dot{m}_{02})]
\end{aligned} \tag{23}$$

where the material derivative of kernel function moments is expressed as

$$\begin{aligned}
\dot{m}_{ij}(x,y) = \sum_{I=1}^{\mathrm{NP}}&[i(x - x_I)^{i-1}(V_x - V_x^I)\times \\
&(y - y_I)^j w_d(x,y) + j(x - x_I)^i\times \\
&(y - y_I)^{j-1}(V_y - V_y^I)w_d(x,y) + \\
&(x - x_I)^i(y - y_I)^j\dot{w}_d(x,y)]
\end{aligned} \tag{24}$$

When the design velocities are given, (23) and (24) can be evaluated prior to the sensitivity analysis. We will show below that these explicit expressions for material derivative of shape functions in combination with the above analytical forms of shape functions undoubtedly enhance the process of structural analysis as well as sensitivity analysis. It should be noted that the material derivative of $N_{I,x}$ and $N_{I,y}$ can be expressed as the similar forms as that of $\dot{N}_I$, and the detailed expressions are omitted here.

Substituting approximation (20) into (18) in combination with the approximations given in (9) gives

$$(\mathbf{K} + \mathbf{K}_\alpha)\dot{\mathbf{d}} = \mathbf{F}^\ell - (\mathbf{M} + \mathbf{N})\mathbf{d} \tag{25}$$

where matrices $\mathbf{M}$ and $\mathbf{N}$ and column vector $\mathbf{F}^\ell$ consist of the following submatrices and subvectors

$$\mathbf{M}_{IJ} = \int_\Omega (\mathbf{B}_I^{\mathrm{T}}D\dot{B}_J + \mathbf{B}_I^{V\mathrm{T}}DB_J + \mathbf{B}_I^{\mathrm{T}}\mathbf{D}\mathbf{B}_J\mathrm{div}\mathbf{V})\mathrm{d}\Omega \tag{26}$$

$$\mathbf{N}_{IJ} = \alpha \int_{\Gamma_u} [\Phi_I^{\mathrm{T}} S \dot{\Phi}_J + \Phi_I^{\mathrm{T}} \mathbf{S} \Phi_J (\mathbf{V} \cdot \mathbf{n}) H] \mathrm{d}\Gamma \tag{27}$$

$$\mathbf{F}_I^{\ell} = \int_{\Omega} \Phi_I^T [\dot{b} + \mathbf{b} \mathrm{div} \mathbf{V}] \mathrm{d}\Omega + \int_{\Gamma_t} \Phi_I^{\mathrm{T}} [\dot{\bar{t}} + \bar{\mathbf{t}} (\mathbf{V} \cdot \mathbf{n}) H] \mathrm{d}\Gamma + \alpha \int_{\Gamma_u} \Phi_I^T S \bar{u} (\mathbf{V} \cdot \mathbf{n}) H \mathrm{d}\Gamma \tag{28}$$

in which

$$\dot{\mathbf{B}}_I = \begin{bmatrix} \dot{N}_{,x}^I & 0 & \dot{N}_{,y}^I \\ 0 & \dot{N}_{,y}^I & \dot{N}_{,x}^I \end{bmatrix}^{\mathrm{T}},$$

$$\mathbf{B}_I^V = -\begin{bmatrix} N_{,k}^I V_{k,x} & 0 & N_{,k}^I V_{k,y} \\ 0 & N_{,k}^I V_{k,y} & N_{,k}^I V_{k,x} \end{bmatrix}^{\mathrm{T}}$$

In the expression of $\mathbf{B}_I{}^V$, summation over repeated indices is implied.

It should be pointed out that the left-hand side matrices involved in (25) are the same as that appear in (10). Therefore, only the calculation of the matrices in the right-hand side of (25) is needed. Once $\dot{d}$ is obtained, it is substituted into (20) to compute the sensitivity of displacement and ultimately to evaluate the sensitivities of strain and stress by the corresponding strain measure and the constitutive law.

3.3 Discretizing of design sensitivity equation by the Bobaru's approach

As an alternative to (20), Bobaru and Mukherjee (2001) presented, considering $\dot{u}$ an ordinary smooth field variable and treating $\dot{u}$ in the standard discretization manner, another discretization approach as follows

$$\dot{u} = \sum_{I=1}^{\mathrm{NP}} N^I \hat{\dot{d}}^I \tag{29}$$

Note that a hat is superposed on $\hat{\dot{d}}^I$ to indicate that it is different from $\dot{d}$ in (20). Actually, it is considered here that $\hat{\dot{d}}^I$ contains not only the information of $\dot{d}$ but also the information of $\dot{N}^I \mathbf{d}^I$ in (20). Substituting the expression (29) and invoking the following relationships,

$$\varepsilon(\mathbf{u}) = \mathbf{B}\mathbf{d},\ \varepsilon(\eta) = \mathbf{B}\bar{\mathbf{d}},\ \sigma(\mathbf{u}) = \mathbf{D}\mathbf{B}\mathbf{d},\ \sigma(\dot{\mathbf{u}}) = \mathbf{D}\mathbf{B}\hat{\dot{\mathbf{d}}}$$

it follows that

$$(\mathbf{K} + \mathbf{K}_{\alpha})\hat{\dot{\mathbf{d}}} = \hat{\mathbf{F}}^{\ell} - (\hat{\mathbf{M}} + \hat{\mathbf{N}} + \hat{\mathbf{N}}^{\mathrm{T}})\mathbf{d} \tag{30}$$

As counterparts of 26–28, we have

$$\hat{\mathbf{M}}_{IJ} = \int_{\Omega} \mathbf{B}_I^{\mathrm{T}} \mathbf{D} \mathbf{B}_J \mathrm{div} \mathbf{V} \mathrm{d}\Omega + \alpha \int_{\Gamma_u} \Phi_I^{\mathrm{T}} \mathbf{S} \Phi_J (\mathbf{V} \cdot \mathbf{n}) H \mathrm{d}\Gamma \tag{31}$$

$$\hat{N}_{IJ} = \int_{\Omega} \mathbf{B}_I^{\mathrm{T}} \mathbf{D} \mathbf{B}_J^V \mathrm{d}\Omega \tag{32}$$

$$\hat{F}_I^{\ell} = \int_{\Omega} \Phi_I^{\mathrm{T}} [\mathbf{b} + \mathbf{b} \mathrm{div} \mathbf{V}] \mathrm{d}\Omega + \int_{\Gamma_t} \Phi_I^{\mathrm{T}} [\dot{\bar{t}} + \bar{\mathbf{t}} (\mathbf{V} \cdot \mathbf{n}) H] \mathrm{d}\Gamma + \alpha \int_{\Gamma_u} \Phi_I^{\mathrm{T}} \mathbf{S} \bar{\mathbf{u}} (\mathbf{V} \cdot \mathbf{n}) H \mathrm{d}\Gamma \tag{33}$$

3.3.1 Remark

In the Kim's discretization approach, the sensitivity of displacement is decomposed into two parts: one consists of material derivative of nodal parameters while another consists of explicit variations of meshless shape functions with respect to shape design variations. This approach is more consistent in the sense of discretization, and, furthermore, highlights the differences between the meshless shape functions and the shape functions of the FEM. Boburu's approach provides alternative appealing discretization scheme for practical application. From the viewpoint of application, Bobaru's approach is more realistic and simpler because it avoids the complexities involved in calculating the material derivative of shape functions and thus simplifies the implementation of shape DSA. Although these two discretization approaches are seemingly different and lead to different implementation of DSA using meshless method, it should be pointed out that these two discretization approaches are equivalent, and any of them can give correct answers as shown in the following numerical examples. The choice of discretization scheme is only a matter of preference.

4 Numerical examples

In order to prove the effectiveness of enhanced RKPM for DSA and to demonstrate the equivalence of two discretization approaches, two 2D linear elasticity examples given in Bobaru and Mukherjee 2001 are adopted, in which the analytical solutions of sensitivities are available. The two examples are the pulling of a bar and the Lame's problem, and denoted by numerical examples 1 and numerical example 2, respectively. As state previously, the enhanced RKPM will accelerate structural responses analysis as well as the DSA.

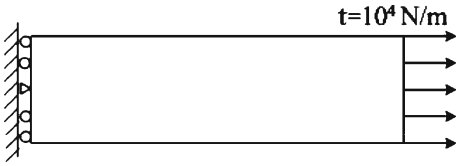

Fig. 1 Numerical example 1: the pulling of a bar

In addition, the Bobaru's discretization approach is simpler to be implemented. It is desirable to perform shape optimization by combing the improved RKPM and the Bobaru's approach. This is demonstrated via a portal frame optimization problem.

4.1 Numerical example 1: the pulling of a bar

The same parameters as given in Bobaru and Mukherjee 2001 are used in this paper: a bar of dimensions 5 m×20 m with Young's modulus of $E=3\times10^7$ N/m^2 and Poisson's ratio $\gamma=0.3$ is chosen as the computational model as shown in Fig. 1. A traction $t=10^4$ N/m^2 is applied at the right end of the bar, while the left end of the bar is fixed. The penalty parameter is chosen as $\alpha=10^6\times E$. The design variable is chosen to be the length of the bar. The exact solutions of displacement sensitivities in the x and y directions are (Bobaru and Mukherjee 2001):

$$\dot{u}_x(X,\tau)=\varepsilon_{11}\frac{x}{l},\ \dot{u}_y(X,\tau)=0$$

The displacement sensitivity in the x direction given by using two discretization approaches are compared with the exact solutions given above and illustrated in Figs. 2 and 3, respectively.

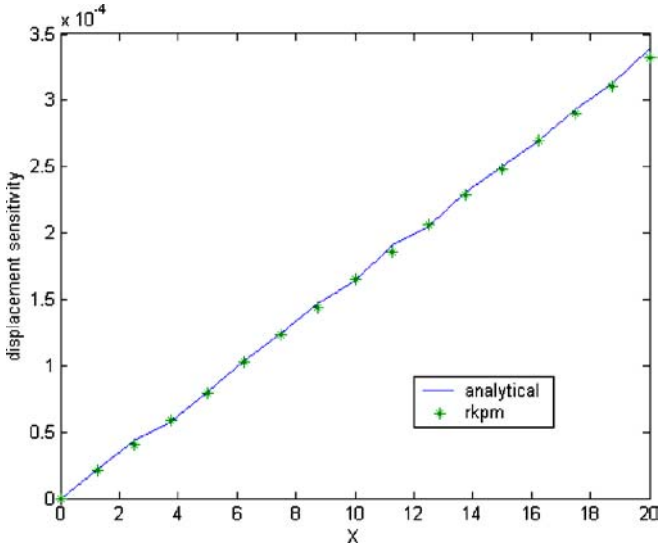

Fig. 2 Comparison of analytical displacement sensitivity to numerical results by Kim's discretization approach

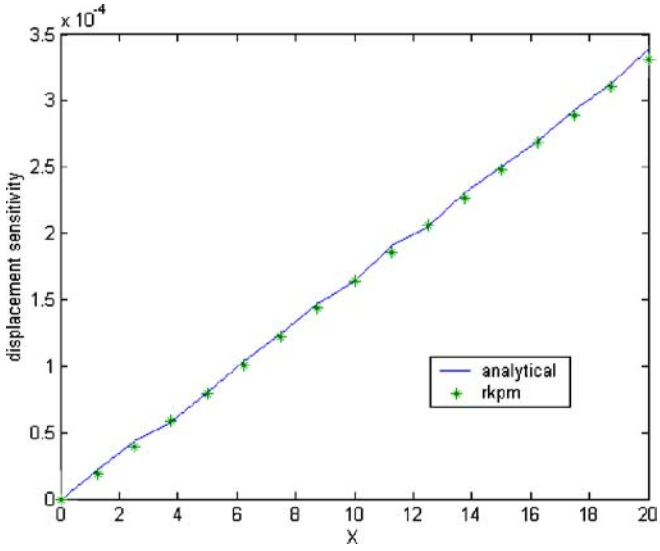

Fig. 3 Comparison of analytical displacement sensitivity to numerical results by Bobaru's discretization approach

4.2 Numerical example 2: Lame's problem

The second example chosen here is the Lame's problem. A cylinder of internal radius $a=1$ and external radius $b=2$ is subjected to uniform internal pressure $p=1$ as shown in Fig. 4. We take $E=1$, $\gamma=0.3$ and $\alpha=10^6\times E$ as computation parameters for this problem. Choosing the internal radius as the design variable and a liner design velocity field, the exact

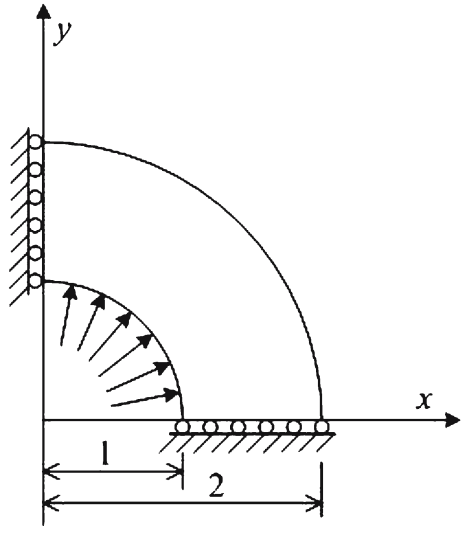

Fig. 4 Numerical example 2: Lame's problem

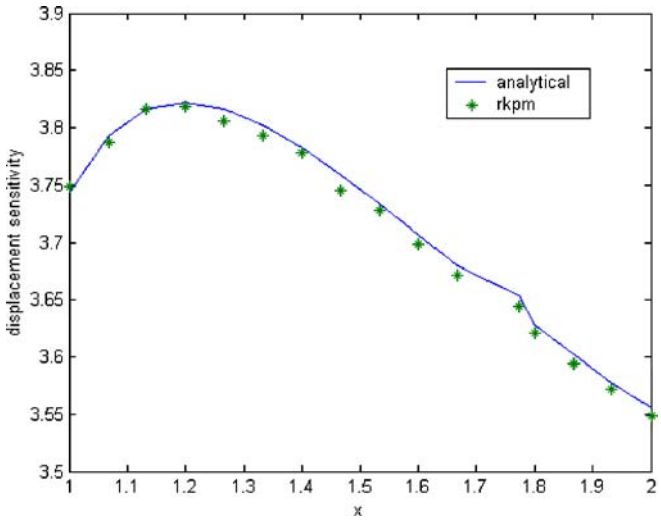

Fig. 5 Comparison of analytical displacement sensitivity to numerical results by Kim's discretization approach

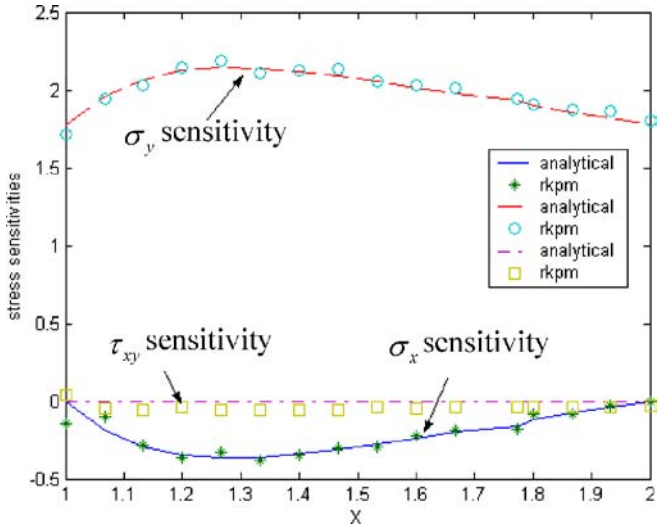

Fig. 7 Comparison of analytical stress sensitivity to numerical results by Kim's discretization approach

expressions of sensitivities of displacement and stress have the following form in the polar coordinates:

$$\dot{u}_x = \dot{u}_r \cos\theta$$
$$\dot{u}_y = \dot{u}_r \sin\theta$$
$$\dot{\sigma}_{rr} = \frac{2ab^2 p[r(r^2-b^2)+a(b-r)(b+a)]}{(b^2-a^2)^2 r^3}$$
$$\dot{\sigma}_{\theta\theta} = \frac{2ab^2 p[r(r^2+b^2)-a(b-r)(b+a)]}{(b^2-a^2)^2 r^3}$$
$$\dot{\sigma}_{r\theta} = 0$$

where

$$\dot{u}_r = \frac{2pab^2}{E(b^2-a^2)^2}\left[(1-\gamma)r + (1+\gamma)\frac{b^2}{r}\right] + \frac{pa^2(b-r)}{E(b^2-a^2)(b-a)}\left[(1-r)-(1+r)\frac{b^2}{r^2}\right]$$

The comparison of exact results and numerical results of displacement and stress sensitivities for the points on the x-axis is made and shown in Figs. 5, 6, 7, and 8. The numerical results are given by using two discretization approaches.

From Figs. 2, 3,and Figs. 5, 6, 7, and 8, we come to the conclusion that RKPM is effective for shape DSA, and it can provide numerical results with great accuracy as compared with the exact solutions. Furthermore, a prior conclusion, which can be drawn from these figures, is that both of these two discretization approaches are definitely correct, and they are intrinsically equivalent.

4.3 The effectiveness of the enhanced RKPM for DSA

To demonstrate the effectiveness of the enhanced RKPM for shape DSA, the computation time of two numerical examples

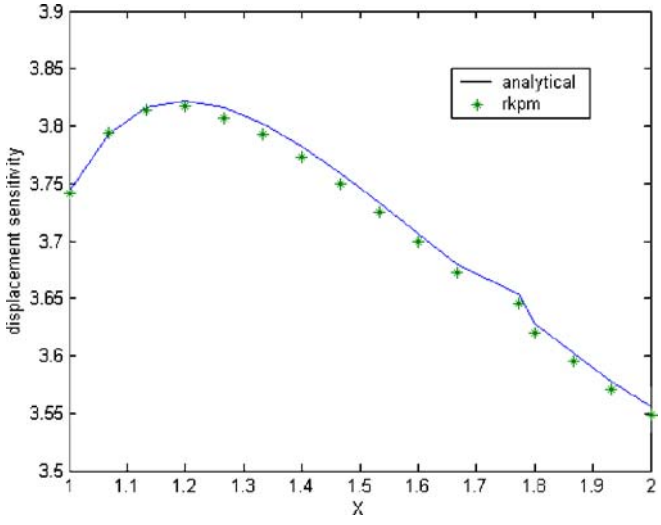

Fig. 6 Comparison of analytical displacement sensitivity to numerical results by Bobaru's discretization approach

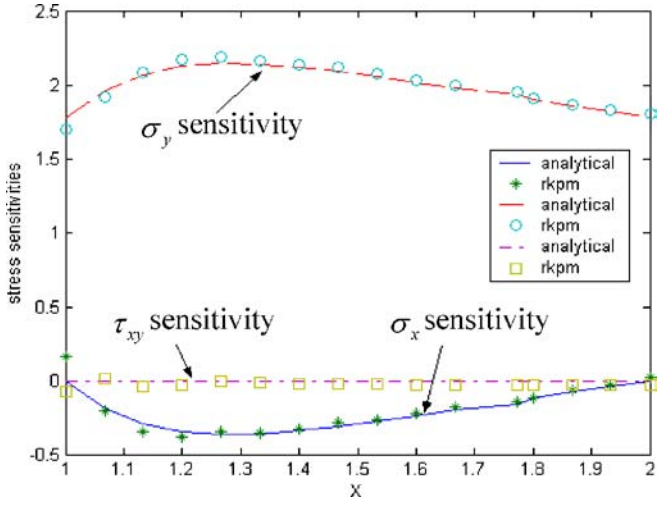

Fig. 8 Comparison of analytical stress sensitivity to numerical results by Bobaru's discretization approach

Table 1 Comparison of computation time of DSA between classical and enhance RKPM (unit of time: min)

Numerical examples	Classical RKPM	Enhanced RKPM
Numerical example 1 (particle number: 85)	17	7
Numerical example 1 (particle number: 256)	56	24

exhausted by classical RKPM and the proposed enhanced RKPM is compared and presented in Table 1. The particle numbers of examples 1 and 2 are 85 and 256, respectively. The computer used here is a PIII 800 PC computer. As can be seen from Table 1, the enhanced RKPM proposed in this paper can markedly speed up the process of shape DSA. The time-savings of enhanced RKPM is nearly 70% of the computation time of classical RKPM as for the presented two examples.

4.4 Shape optimization of a portal frame by enhanced RKPM

The computational model is shown in Fig. 9, in which AB, CD, DE, and FG are four boundaries to be optimized. A total of 14 design variables are chosen to be the x-coordinates of five key points on AB and FG, and the x-coordinates of two key points on CD and DE, respectively. The objective is to minimize the area of the frame under the constraint that the von Mises stress does not exceed the admissible stress—300 MPa in this paper. Material constants with E= 207 MPa and γ=0.3 are assumed. A total of 496 particles are used to discretize the domain. After eight optimization iterations, a 23.7% area reduction from initial 9,055 mm^2 to final 6,908 mm^2 is obtained. Figure 10 shows the final particle distribution, and Fig. 11 shows the final non Mises stress distribution after eight optimization iterations, respectively.

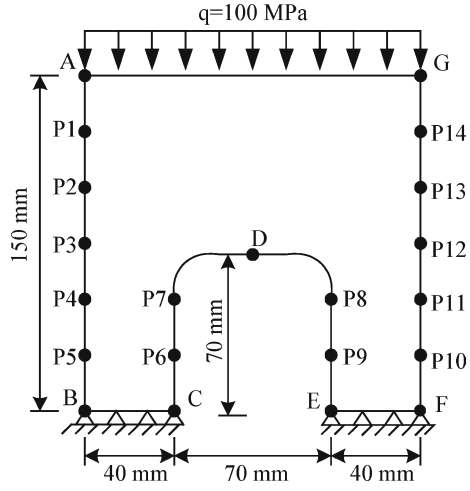

Fig. 9 Computation and optimization model of a portal frame

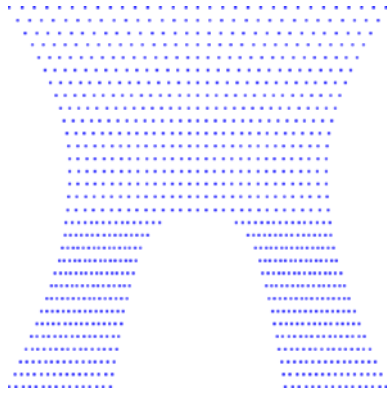

Fig. 10 Final particle distribution after eight iterations

5 Concluding remarks

RKPM is implemented in a different manner such that RKPM shape functions and their derivatives are expressed explicitly in terms of kernel function moments. The analogous ideas are followed in the shape DSA formulations, in which the material derivative of shape functions is also written analytically in terms of material derivative of moments. The goal of these efforts is to provide explicit forms of RKPM shape functions for programming, and the matrix inversions or solutions of linear systems are absolutely eliminated. This lead to marked time reduction in structural analysis and shape DSA and, at last, we believe, can speed up the process of shape optimization and make RKPM more realist and applicable. The effectiveness of enhanced RKPM is proved via two 2D linear elasticity problems, and it is shown that the computation time decrease is more than 50% of that of classical RKPM.

Discretization scheme is an important issue from the point of view of practice, and it is another topic in this paper. Using meshless methods for DSA, there exist two superficially different discretization approaches, called Kim's approach and Bobaru's approach herein, for Galerkin approximation

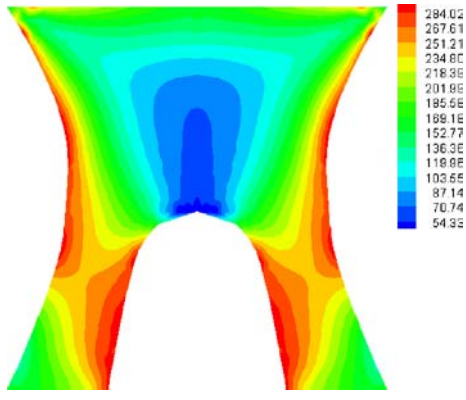

Fig. 11 Final von Mises stress contour after eight iterations

of shape sensitivity equation, which is a key equation for shape DSA. It is demonstrated through numerical examples that these two discretization approaches are equivalent, and both of them can give correct results. Kim's approach is more consistent in the sense of discretization, while Bobaru's approach is simpler and more appealing in practice. The choice of discretization approach is a matter of taste.

Finally, a more complicated portal frame shape optimization problem with four design boundaries is studied by an integration of the enhanced RKPM into Baboru's approach. This example demonstrates the feasibility and the effectiveness the improvements and efforts made in this paper. The developments and applications of these improvements to shape optimization problems of nonlinear structures undergoing large deformation by meshless method are underway.

Acknowledgements This research is funded by National Natural Science Foundation of China under grant number 10202018. The second author is also grateful to Dr. Bobaru for his helpful discussions, for this paper is motivated by the discussions with Dr. Bobaru. Thanks are also due to Mr. W. Zou for preparing some numerical examples.

References

Atluri SN, Zhu T (2000) New concepts in meshless methods. Int J Numer Methods Eng 47:537–556

Belytschko T, Lu YY, Gu L (1994) Element-free Galerkin methods. Int J Numer Methods Eng 37:229–256

Belytschko T, Krongauz Y, Organ D, Fleming M, Krysl P (1996) Meshless methods: an overview and recent developments. Comput Methods Appl Mech Eng 139:3–47

Bobaru F, Mukherjee S (2001) Shape sensitivity analysis and shape optimization in planar elasticity using the element-free Galerkin method. Comput Methods Appl Mech Eng 190:4319–4337

Duarte CA, Oden JT (1995) HP clounds—a meshless method to solve boundary-value problems. Technical Report 95-05. Texas Institute for Computational and Applied Mathematics, University of Texas at Austin

Grindeanu I, Chang KH, Choi KK, Chen JS (1998) Design sensitivity analysis of hyperelastic structures using a meshless method. AIAA J 36:618–627

Haftka RT, Grandhi RV (1986) Structural shape optimization—a survey. Comput Methods Appl Mech Eng 57:91–106

Haug EJ, Choi KK, Komkov V (1986) Design sensitivity analysis of structural systems. Academic, New York, NY

Kim NH, Choi KK, Chen JS, Park YH (2000a) Meshless shape design sensitivity analysis and optimization for contact problem with friction. Comput Mech 25:157–168

Kim NH, Choi KK, Chen JS (2000b) Shape design sensitivity analysis and optimization of elasto-plasticity with frictional contact. AIAA J 38:1742–1753

Kim NH, Park YH, Choi KK (2001) Optimization of a hyper-elastic structure with multibody contact using continuum-based shape design sensitivity analysis. Struct Multidiscipl Optim 21:196–208

Kim NH, Choi KK, Botkin ME (2003) Numerical method for shape optimization using meshfree method. Struct Multidiscipl Optim 24:418–429

Li S, Liu WK (2002) Meshfree and particle methods and its applications. ASME Appl Mech Rev 55:1–34

Liu WK, Jun S, Zhang YF (1995) Reproducing kernel particle methods. Int J Numer Methods Eng 20:1081–1106

Liu WK, Chen Y, Jun S, Chen JS, Belytschko T, Pan C, Uras RA, Chang CT (1996) Overview and applications of the reproducing kernel particle methods. Arch Comput Methods Eng: State-of-the-Art-Rev 3:3–80

Melenk JM, Babuska I (1999) The partition of unity finite element method: basic theory and applications. Comput Methods Appl Mech Eng 139:289–314

Zhou JX, Wang XM, Zhang ZQ, Zhang L (2005) Explicit 3-D RKPM shape functions in terms of kernel function moments for accelerated computation. Comput Methods Appl Mech Eng 194:1027–1035